Mechanical and thermal properties of graphene sulfonate nanosheet reinforced sacrificial concrete at elevated temperatures

Hong-yan Chu [a, b], Jin-yang Jiang [a, b*], Wei Sun [a, b], Mingzhong Zhang [c†]

[a] School of Materials Science and Engineering, Southeast University, Nanjing 211189, China

[b] Jiangsu Key Laboratory of Construction Materials, Nanjing 211189, China

[c] Advanced and Innovative Materials (AIM) Group, Department of Civil, Environmental and Geomatic Engineering, University College London, London WC1E 6BT, UK

Abstract: Progress in the field of nanomaterials presents an opportunity to improve the performance of cementitious composites via graphene or its derivatives. This paper presents an experimental study on mechanical and thermal properties of sacrificial concrete without and with graphene sulfonate nanosheets (GSNSs) during high temperature exposure. The microstructure, porosity, mechanical strengths, thermal analysis, coefficient of thermal expansion, thermal diffusivity and ablation behaviour of sacrificial concrete during exposure to various temperatures up to 1000 ℃ were comprehensively investigated. Two new experimental apparatuses were developed and used to measure mechanical strengths of sacrificial concrete at elevated temperatures. It was found that the compressive strength, splitting tensile strength, thermal diffusivity and decomposition enthalpy of sacrificial concrete were increased by 12.98-25.36%, 8.66-34.38%, 25.00-103.23% and 4.23% respectively when adding 0.1 wt% GSNSs, while the porosity and ablation velocity of sacrificial concrete were reduced by 3.01-6.99% and 4.14% respectively due to the incorporation of GSNSs.

Keywords: sacrificial concrete; graphene nanosheet; mechanical strength; thermal analysis; microstructure

1. Introduction

---

[*] Corresponding author. Tel.: +86-025-52090667; E-mail address: jiangjinyang16@163.com (J.-y. Jiang)

[†] Corresponding author. Tel.: +44 020 7679 7299; E-mail address: mingzhong.zhang@ucl.ac.uk (M. Zhang)

Cementitious composites are the most important and widely used civil engineering materials. Recent progress in the field of nanotechnology has provided an opportunity to improve the performance of cementitious composites by incorporating nano-sized materials, such as nano-SiO_2 [1-3], nano-TiO_2 [4], nano-Al_2O_3 [5, 6], nano-Fe_3O_4 [7] and carbon nanotubes [8-10]. When small particles were evenly distributed in cementitious materials, they served as nucleation sites, as a result of which the degree of cement hydration can be improved [11]. In addition, the nanomaterials contribute to the microstructural regulation of cement composites and the microstructure of cementitious materials can be improved significantly by adding nanomaterials [12], and nanomaterial has nano-filler effect on cementitious materials [13].

Nowadays, graphene as a new kind of nanomaterial has attracted a lot of interest. Graphene manifests a single atom thickness of 2D carbon atoms planar sheet with sp^2 bonded pattern and has distinguished optical, electrical, thermal and mechanical properties [14]. The electrical conductivity, thermal conductivity, tensile strength and elastic modulus of graphene are 2000 S/cm, 5300 W/mK, 130 GPa and 1 TPa [15-17], respectively. The specific surface area of one single graphene sheet is 2630 m^2/g [16]. Because of its excellent properties, graphene has a promising prospect when combined with cementitious composites. However, the use of graphene is still hampered by its poor water dispersing ability and high production cost. As derivatives of graphene, graphene nanosheets (GNSs) and graphene oxide nanosheets (GONSs) are also carbon nanomaterials composed of graphene stacks or graphene sheets [18-21]. GONSs are oxides of GNSs and contain oxygen functional groups that attach on the basal plans and edges of graphene oxide sheets. The functional groups can modify the van der Waals interactions between the GONSs and thus lead to the improvement of the water dispersing capability of GONSs [22]. Moreover, the GNSs and GONSs are lower-cost nanomaterials as compared to graphene.

So far, an increasing number of studies have been conducted to investigate the influence of graphene or its derivatives on properties of cementitious composites. Horszczruk et al. [23] reported that the Young's modulus of cement paste was significantly enhanced by adding 3 wt% graphene oxide. Bulut [24] explored the effect of graphene nanopellets on mechanical properties of basalt/epoxy composites and found that the mechanical properties of basalt/epoxy composites could be significantly improved due to the addition of 0.1 wt% graphene nanopellets. Murugan et al. [25] observed that the addition of 0.02 wt% GONS by weight of cement can lead to an increase of up to 70% and 23% respectively in the 7-day and 28-day flexural strength of cement paste. Lu et al. [26] concluded that the compressive strength and flexural strength of cement paste were increased by 11.05% and 16.20%, respectively, when adding 0.05 wt% graphene oxide. Apart from enhancing mechanical properties, the self-sensing ability of cementitious materials can also be improved due to the addition of conductive nanomaterials. Le et al. [20] found that the GNSs could be used to characterise the damage in cement composites due to their extraordinary electrical conductivity. The self-sensing ability of GNSs reinforced cement composites was found to be similar to the self-induction of carbon fibre reinforced conductive concrete [27]. Although a great deal of research has been conducted on cement paste or mortar reinforced with graphene or its derivatives, there are only few investigations of the use of them in concrete. In addition, there is no publication devoted to properties of graphene sulfonate nanosheets (GSNSs) reinforced concrete. Compared to GONSs, the production cost of GSNSs is lower. The sulfonic groups contained in GSNSs are similar to that of hydroxyl functional (–OH) groups in GONSs, thus the GSNSs may also be used to improve the properties of cementitious materials.

As a key component of European Pressurized Water Reactor, sacrificial concrete is designed to reduce the leakage potential of radioactive materials in severe nuclear accidents through its encasing

function [28]. Ferro-siliceous sacrificial concrete and siliceous sacrificial concrete are the two most widely used sacrificial concrete. On one hand, sacrificial concrete can melt and mix with corium (a molten mixture of fuel material, partially or totally oxidized cladding, non-volatile fission products and various structural materials) reducing the temperature of corium. On the other hand, the SiO_2 from sacrificial concrete can oxidize Zr in the corium and the glassily matrix formed by molten SiO_2 can enwrap the radioactive fission products [29]. In case of fire or nuclear accident, concrete is exposed to elevated temperatures. Although extensive research on the behaviour of concrete subjected to high temperatures has been reported so far [30-34], investigation on the thermal properties of sacrificial concrete is rare, especially on its mechanical properties during elevated temperature exposure. Chu et al. [35] have recently carried out a systematic study on mechanical and physicochemical properties of ferro-siliceous sacrificial concrete after high temperature exposure, and observed that the compressive strength-ultrasonic pulse velocity (UPV) and splitting tensile strength-UPV relationships followed a Weibull distribution and was in exponential form, respectively. It is worth pointing out that the mechanical properties of concrete during high temperature exposure and after exposure (i.e., concrete has been cooled down) are different, as the damage due to elevated temperatures can be retrieved during cooling. Overall, only very little information is available on the properties of sacrificial concrete at high temperatures. Moreover, the effects of GSNSs on thermal and mechanical properties of sacrificial concrete have rarely been studied elsewhere.

The main purpose of this paper is to investigate the mechanical and thermal properties of sacrificial concrete without and with GSNSs before and during high temperature exposure, which extends authors' recently published work [36] from siliceous sacrificial concrete to ferro-siliceous sacrificial concrete. Two new experimental facilities for measuring the compressive strength and splitting tensile strength of sacrificial concrete during elevated temperature exposure are developed. Afterwards, a

series of experiments were carried out to estimate the microstructure, porosity, compressive strength, splitting tensile strength, thermal analysis, coefficient of thermal expansion (CTE), thermal diffusivity and ablation behaviour of sacrificial concrete without and with GSNSs before and at different temperatures, i.e., 200, 400, 600, 800, and 1000 ºC.

2. Experimental programme

2.1 Materials

Silica fume and Class I fly ash (equivalent to ASTM C 618 Class F fly ash) were used as supplementary cementitious materials in the study. The chemical composition of cement and supplementary cementitious materials are shown in Table 1. The specific gravity of cement and silica fume was 3.15 and 2.22, respectively. The specific surface of cement and silica fume was 362.20 m^2/kg and 2.79×10^4 m^2/kg, respectively. The compressive strength of cement mortar (water/cement/sand = 1:2:6) at 28 days was 62.8 MPa.

Silica sand and iron ore supplied by Nuclear Industry Nonmetallic Mineral Powders Co., Ltd (Liuzhou, China) and Nuclear Science and Technology Co., Ltd (Tongchang, China) respectively were used as aggregates. The silica sand was composed of SiO_2, $CaCO_3$, and $MgCO_3$, the weight percentages of which were 99.88%, 0.058%, and 0.062%, respectively. The iron ore contained 92.22 wt% Fe_2O_3, 7.61 wt% SiO_2, and 0.17 wt% $CaCO_3$. Table 2 shows the sieve analysis of aggregates.

A superplasticizer of polycarboxylate supplied by Sobute New Materials Co., Ltd (Nanjing, China) was used to gain a satisfactory fluidity of sacrificial concrete. The solid content and water-reducing rate of superplasticizer were 40.0 wt% and 33.9%, respectively. The physical and mechanical properties of polypropylene fibre used in this work are presented in Table 3. The graphene sulfonate solution was obtained from Graphene-Tech Co., Ltd (Suzhou, China). The solid content, particle size, and thickness of GSNSs were 10.5 wt%, 50-100 μm, and 1-2 nm, respectively.

2.2 Specimen preparation

Table 4 shows the mixtures of sacrificial concrete that were carefully designed in accordance with our previous research findings shown in literature [28] and further improved via the addition of GSNSs. Herein, the ferro-siliceous sacrificial concrete mixtures without and with GSNSs were marked as FC and FCG, respectively. The content of GSNSs in the FCG mixture was 0.1 wt% of binders (cement and supplementary cementitious materials).

Based on the above mixtures, the cubic specimens (150×150×150 mm) of sacrificial concrete were cast. After casting, the molds were covered with plastic sheets and were cured for 24 h at ambient conditions. Afterwards, the molds were removed and the specimens were cured in a standard curing room (21±1 ℃ and relative humidity of above 95%) for 28 days. In total, 60 cubic specimens were prepared for each mixture. It should be highlighted that, in order to obtain a homogeneous mixture, the polypropylene fibre was dispersed carefully by hand, and then mixed with cement, silica sand and iron ore using a mixer for 5 min. Meanwhile, the GSNSs solution was mixed with superplasticizer, and a part of water was subsequently poured into the mixture and stirred evenly. Afterwards, the mixed solution was added to the dry materials and mixed in the mixer for another 5 min. Note that the rest of water was firstly used to flush the mixed solution container, before it was added to the mixer.

2.3 Test methods

2.3.1 Microstructure

To detect the microstructure of sacrificial concrete without and with GSNSs, a FEI 3D environmental scanning electronic microscopy (ESEM) was used. The micrographs of specimens were taken at ambient temperature and after exposure to high temperatures, i.e., 200, 400, 600, 800, and 1000 ℃.

2.3.2 Porosity

A Micromeritics AutoPore Ⅳ 9510 mercury intrusion porosimetry (MIP) was used to estimate the pore evolution of sacrificial concrete without and with GSNSs at elevated temperatures.

2.3.3 Mechanical properties

Fig. 1 shows the two new experimental facilities that were developed to measure the compressive strength and splitting tensile strength of sacrificial concrete without and with GSNSs during elevated temperature exposure.

The compressive strength measuring equipment consists of a universal testing machine and an electrical furnace. The outline of the universal testing machine with a maximum load capacity of 3000 kN is composed of steel columns and beams. The top and bottom blocks of the machine are made of a high temperature resistant material that still has high strength and stiffness at 1200 ℃. The red frame in Fig. 1a denotes the electrical furnace, the heating rate and maximum temperature of which are 0.5-15 ℃/min and 1500 ℃, respectively. The furnace is bigger enough to hold three padding blocks on the slide rail and there is an electric actuator to push the padding blocks along the track, thus the compressive strength of three specimens can be measured at a time. The silicon carbide rods are distributed evenly on the side walls of furnace. A thermocouple is installed at the middle of furnace to monitor the temperature of furnace chamber. There are two displacement measuring bars made of a high temperature resistant material that has rather small coefficient of thermal expansion: one is on the top of padding block; the other is on the top of the steel plate with a thickness of 4 mm between the upper surface of specimen and the downward surface of top bearing block. Two grating displacement sensors with a precision of ±1 μm connect with two displacement measuring bars, respectively, such that the deformation of specimen during the compression test can be obtained accurately. In addition, there are cooling systems on the top and bottom blocks of universal testing

machine and electric actuator. The cooling is achieved by letting the cool water flow through the cooling systems.

Similarly, the splitting tensile strength measuring apparatus is also composed of a universal testing machine and an electrical furnace, as shown in Fig. 1b. The universal testing machine, electrical furnace, displacement measuring bars and cooling systems in the splitting tensile strength measuring apparatus are the same as those used in compression test except those: the maximum load capacity of the universal testing machine is 300 kN and the displacement measuring bars are on the left and right sides of furnace.

In this work, the specimens were heated from ambient temperature, i.e., 25 ℃ to 200, 400, 600, 800, and 1000 ℃ at a heating rate of 5 ℃/min. According to literature [34], the specimens were held at the target temperature for 2 h in order to ensure a uniform temperature throughout each specimen. After that, the compressive strength and splitting tensile strength of specimens before and during high temperature exposure were measured using the developed two new experimental facilities with a loading rate of 0.3 MPa/s and 0.03 MPa/s, respectively.

2.3.4 Thermal analysis

Thermogravimetric analysis (TGA) and differential scanning calorimetry (DSC) of sacrificial concrete without and with GSNSs were performed via a simultaneous thermal analyzer (NETZSCH STA449 F3). The experimental conditions were: at standard atmospheric pressure, in nitrogen circumstance and at the heating rate of 10 ℃/min up to 1300 ℃. The specimen used in the TGA experiment was ground into power by hand using an agate mortar.

2.3.5 Coefficient of thermal expansion

A dynamic thermal mechanical analyzer (NETZSCH TMA402 F1) was used to measure the thermal deformation of sacrificial concrete at elevated temperatures. The thermal deformation of

sacrificial concrete without and with GSNSs was carried out in accordance with ASTM E 831-03 on 8×8×20 mm prismatic specimens that were sliced from the 150×150×150 mm specimens. The linear variation in length of each specimen was measured by the device at a heating rate of 10 ºC/min. The relationship between thermal strain and CTE can be determined as follows

$$\varepsilon = \Delta L / L_0 \tag{1}$$

$$\Delta L = \alpha \cdot L_0 \cdot \Delta T \tag{2}$$

where ε is the thermal strain, ΔL is the unit length change, L_0 is the initial length of the specimen, α is the CTE and ΔT is the temperature difference.

Substituting Eq. (2) to Eq. (1), the relationship between thermal strain and CTE can be derived as

$$\varepsilon = \alpha \cdot \Delta T \tag{3}$$

As such, the CTE of sacrificial concrete between ambient temperature (25 ºC) and each target temperature (200, 400, 600, 800 and 1000 ºC) can be calculated using Eq. (3).

Assume that sacrificial concrete is a homogeneous material, the relationship between its volumetric CTE β and linear CTE α can be expressed as

$$\beta = 3\alpha \tag{4}$$

2.3.6 Thermal diffusivity

The thermal diffusivity of a material is defined as the ratio of the heat transmitted to the heat stored by unit mass of the material, as seen in Eq. (5). In steady or quasi-steady states, the heat transmission through conduction is controlled by thermal diffusivity.

$$a = \lambda / (c \cdot \rho) \tag{5}$$

where a is the thermal diffusivity, λ is the thermal conductivity, c is the specific heat and ρ is the density of sacrificial concrete.

The thermal conductivity and specific heat of sacrificial concrete before and during high

temperature exposure (25, 200, 400, 600, 800, and 1000 ºC) were measured by a laser thermal constant analyzer (NETZSCH LFA457) in accordance with ASTM E 1461-13. The laser flash source was Neodymium-doped gadolinium gallium garnet crystal with a radiant pulse energy up to 18.5 J. The temperature evolution of specimen was detected by an advanced non-contact infrared detector. The specimen size used in the experiment was 10×10×1 mm. The initial density (ρ_0) of sacrificial concrete was determined according to the Chinese standard GB/T 50080-2002 and can be expressed as

$$\rho_0 = \frac{m_0}{V_0} \tag{6}$$

where m_0 and V_0 represent the initial mass and initial volume, respectively.

The density of sacrificial concrete during high temperatures ρ^T can be calculated using the following equation

$$\rho^T = \frac{m^T}{V^T} = \frac{(1-\gamma)m_0}{(1+\beta)V_0} = \frac{(1-\gamma)}{(1+\beta)}\rho_0 \tag{7}$$

where γ is the mass loss ratio of sacrificial concrete.

Based on the results of TGA experiment, the mass loss ratio of sacrificial concrete during high temperature exposure can be determined. Accordingly, the density of sacrificial concrete at high temperatures can be calculated with Eq. (7). Afterwards, the thermal diffusivity of sacrificial concrete before and during elevated temperature exposure can be obtained.

2.3.7 Ablation behaviour

Based on the theory of heat transfer, the ablation velocity (υ) of sacrificial concrete is associated with the heat flux ($\dot{Q}$) through sacrificial concrete and their relationship can be expressed by

$$\upsilon = \frac{\dot{Q}}{\rho \cdot A \cdot \Delta H} \tag{8}$$

where ρ, A, and ΔH denote the density, ablating area and decomposition enthalpy of sacrificial concrete, respectively.

The enthalpy of sacrificial concrete can be estimated by integration of its DSC curve [37]. The zero point of enthalpy is set to 25 ºC here. The decomposition temperature of sacrificial concrete can be determined via a computer-controlled radiant electrically furnace with a heating rate of 5 ºC/min. Subsequently the decomposition enthalpy can be obtained, as such the ablation velocity of sacrificial concrete can be quantified.

It should be mentioned that in order to improve the accuracy of experimental results three repeated measurements were undertaken on the porosity, compressive strength, splitting tensile strength, TGA, DSC, CTE and thermal diffusivity tests at each target temperature. Only the mean values were presented in the work.

3. Results and discussion

3.1 Microstructure

Fig. 2 shows the ESEM images of sacrificial concrete before and after exposure to 25, 200, 400, 600, 800 and 1000 ºC. Initially, the matrix of sacrificial concrete without GSNSs (i.e., FC) presented a continuous microstructure without obvious micro-cracks. At 200 and 400 ºC, a small number of micro-cracks could be observed. More micro-cracks emerged when the temperature reached 600 ºC. At 800 ºC, the micro-cracks connected to each other across the specimen. After exposure to 1000 ºC, the matrix of sacrificial concrete became amorphous and some micro-cracks appeared in the aggregates. The microstructural evolution of sacrificial concrete with GSNSs (i.e., FCG) with increasing temperature was similar to that of FC, as shown in Fig. 2b. However, FCG was more compact than FC at ambient temperature. Two long channels let by molten polypropylene fibres can be observed in FCG at 200 and 400 ºC, and a polypropylene fibre can be found at 200 ºC. This result indicates that some polypropylene fibres in FCG were melted when FCG was exposed to 200 ºC, while the other polypropylene fibres still possessed their initial morphology, although the melting

temperature of the polypropylene fibres used in this work was 169 ºC (see Table 4) and they should be melted after exposure to 200 ºC.

Both the cement paste and aggregate of sacrificial concrete were significantly influenced by elevated temperature due to the pressure induced by moistures and carbon dioxide release [28], and the thermal stress resulting from thermal gradient [38] or thermal incompatibility [39]. Accordingly, the microstructures of sacrificial concrete were gradually damaged as temperature increased, which led to degradation of sacrificial concrete.

It can be seen from Fig. 3a that GSNSs had reinforcing and toughing effects on the microstructure of sacrificial concrete. The yellow square in Fig. 3a was enlarged and presented in Fig. 3b to show details. The cumulate plate-shaped products were clearly observed in Fig. 3b, which indicated that the addition of GSNSs resulted in a denser microstructure of sacrificial concrete. The energy dispersive spectrometer (EDS) analysis was performed on the blue square in Fig. 3b to evaluate the elemental compositions of this area. The main elemental compositions were found to be C, O, Ca, S and Fe, the weight percentages of which were 46.42%, 34.06%, 10.85%, 4.41% and 3.94%, respectively. This result implied that the formation of the cumulative plate-shaped products was because of the addition of GSNSs, because the sulfonic groups in GSNSs might react with hydration products to form covalent bonds, which was similar to poly methyl methacrylate in graphene sheets [40]. Therefore, the GSNSs added to sacrificial concrete could have reinforcing and toughing effects on the microstructure of sacrificial concrete.

3.2 Porosity

Fig. 4 shows the porosity and pore size distribution of sacrificial concrete at ambient temperature and after exposure to 200, 400, 600, 800, and 1000 ºC. With the increase of temperature, the porosity of sacrificial concrete continually increased, which is consistent with the findings for high-strength

concrete subjected to elevated temperatures [41, 42]. The increase of porosity of sacrificial concrete can be attributed to the loss of water in capillary pores and hydration products [43], cracks induced by the incompatible deformation between cement paste and aggregate [39], and the channels due to the melting of polypropylene fibres in sacrificial concrete (see Fig. 2b).

As shown in Fig.4a, the porosity of sacrificial concrete was increased by 26.18% (FC) and 28.97% (FCG), respectively, for temperatures ranging from 25 to 400 ℃. This was followed by a rapid increase in porosity during 400-800 ℃: 128.44% for FC and 130.85% for FCG, which is in consistence with the increasing number of cracks in the microstructure of sacrificial concrete formed in the same temperature range, as seen in Fig.2. Afterwards, there was a gradual increase in porosity of sacrificial concrete when the temperature increased from 800 to 1000 ℃. Compared to that at ambient temperature, the porosity of sacrificial concrete after exposure to 1000 ℃ was increased by 197.29% (FC) and 203.97% (FCG), respectively.

Over the whole range of temperatures, the porosity of FCG was always lower than that of FG. The porosity of FCG was 3.01-6.99% less than that of FG due to the addition of GSNSs, which can be explained by the following two aspects. On one hand, the GSNSs had reinforcing and toughing effects on the microstructure of sacrificial concrete (see Fig. 3b) leading to a reduction in porosity of sacrificial concrete. On the other hand, the thermal gradient in FCG was lower than that of FC due to the addition of GSNSs [38], as a result of which the induced thermal damage in FCG was lower than that in FC.

With regards to pore size distribution, multiple peaks can be observed for temperatures between 25 ℃ and 1000 ℃ and the threshold pore size increased with increasing temperature, as shown in Figs.4b and 4c. At 25, 400 and 800 ℃, most of the pore size of FC were within two peak intervals (0.01, 0.07) μm, (0.08, 2.18) μm, and (0.17, 24.18) μm. There was a similar trend for FCG, but its pore size was

within a smaller range, from 0.01-0.06 μm at 25 ºC, to 0.08-2.13 μm at 400 ºC, to 0.20-23.08 μm at 800 ºC. These results could explain why the porosity of sacrificial concrete increased slowly in the range of 25-400 ºC, while increased rapidly during 400-800 ºC.

3.3 Residual compressive strength

Fig. 5 shows the residual compressive strength and relative residual compressive strength of sacrificial concrete at elevated temperatures that is defined as the ratio of residual compressive strength at elevated temperature to compressive strength at ambient temperature. As seen in Fig.5a, the compressive strength of sacrificial concrete decreased monotonically with the increase of temperature, which is consistent with the change of compressive strength of self-consolidating concrete [31, 44, 45] and siliceous sacrificial concrete [36] exposed to elevated temperatures. The compressive strength loss can be attributed to the increase in porosity of sacrificial concrete over the same range of temperature (see Fig.4a) and to the decrease in both stiffness and cohesive strength of C-S-H gel [46]. In addition, the compressive strength of FCG was always higher than that of FC over the whole range of 25-1000 ºC and the compressive strength of sacrificial concrete was increased by 12.98-25.36% due to the incorporation of GSNSs, which have reinforcing effects. The compressive strength of FCG at 25, 600 and 1000 ºC was, 12.98%, 20.06% and 25.36% higher than that of FC, respectively. The decreasing amplitude of compressive strength for FCG was smaller than that of FC during exposure to elevated temperatures, which can be ascribed to the lower thermal damage in FCG than that in FC at high temperatures due to the addition of GSNSs.

As seen in Fig.5b, the change in relative residual compressive strength of sacrificial concrete against temperature followed a similar trend of that in compressive strength. The relative residual compressive strength of FCG was always higher than that of FC at each target temperature, which indicated that the induced thermal damage FCG was lower than that of FC at high temperatures. At

200 ℃, the relative residual compressive strength of FC and FCG was 84.93% and 87.15%, respectively, which was followed by a sharp drop in the range of 400-600 ℃. The relative residual compressive strength of FC and FCG was only 34.22% and 36.37% at 600 ℃. The relative residual compressive strength kept decreasing with temperature during 800-1000 ℃ and was merely 15.71% (FC) and 17.43% (FCG) at 1000 ℃. Overall, the critical temperature of sacrificial concrete was found to be 400-600 ℃, where the most dramatic decrease in relative residual compressive strength occurred.

3.4 Residual splitting tensile strength

Fig. 6 shows the residual splitting tensile strength and the relative residual splitting tensile strength of sacrificial concrete without and with GSNSs at various temperatures. The relative residual splitting tensile strength is defined as the ratio of residual splitting tensile strength at high temperature to splitting strength at ambient temperature. As seen in Fig.6a, the residual splitting tensile strength of sacrificial concrete declined continually as temperature increased, which is in good agreement with previous studies on siliceous sacrificial concrete [28, 36] and high-strength concrete [47] exposed to elevated temperatures. The decrease in splitting tensile strength of sacrificial concrete was associated with their increasing porosity. The splitting tensile strength of FCG was invariably higher than that of FC due to the addition of GSNSs that resulted in an increase of 8.66-34.38% in the splitting tensile strength of sacrificial concrete. In detail, the splitting tensile strength of FCG at 25, 600 and 1000 ℃ was 8.66%, 21.15% and 34.38% higher than that of FC, respectively.

The relative residual splitting tensile strength of sacrificial concrete decreased monotonically with increasing temperature, as shown in Fig.5b. Similarly, the relative residual splitting tensile strength of FCG was always higher than that of FC at elevated temperatures. There was no obvious drop in the relative residual splitting tensile strength of sacrificial concrete at 200 ℃, that was 86.60% and 87.65% for FC and FCG, respectively. The relative residual splitting tensile strength declined sharply

in the range of 400-600 ºC that is accordance with that for relative residual compressive strength as discussed above. The relative residual splitting tensile strength at 600 ºC was 29.89% (FC) and 33.12% (FCG), respectively. This was followed by a relatively slower decrease in the relative residual splitting tensile strength during 800-1000 ºC, which was only 9.23% (FC) and 11.34% (FCG) respectively at 1000 ºC.

In order to make a direct comparison analysis the relative residual compressive strength and splitting tensile strength of sacrificial concrete at various temperatures were plotted together in Fig. 7. The relative residual compressive strength of sacrificial concrete was found to be higher than the relative residual splitting tensile strength at high temperatures, except for FCG at 200 ºC. For instance, the former was 15.18% (FC) and 18.06% (FCG) respectively higher than the latter at 400 ºC. These results implied that the elevated temperature has a more severe effect on the splitting tensile strength of sacrificial concretes than compressive strength.

3.5 Thermal analysis

Fig. 8 shows the effects of temperature on thermal decomposition (TGA) and heat absorption/desorption (DSC) of sacrificial concrete. As seen in Fig.8a, the weight evolution of FC and FCG was exactly similar, which can be attributed to the nearly same mixtures of them (see Table 4). A quick weight loss can be observed in the TGA for sacrificial concrete in the range of 25-150 ºC, which is consistent with that for self-compacting cement paste subjected to elevated temperatures [48]. The weight loss of sacrificial concrete in this range of temperature can be ascribed to the loss of evaporable water and part of physically bound water. Between 105 ºC and 700 ºC, the mass loss of sacrificial concrete indicated from TGA was associated with the loss of chemically bound water and dehydration of products [49]. At 700 ºC, a significant loss in the weight of sacrificial concrete can be observed, which can be explained by the decarbonation of calcium carbonate. After that temperature,

the curves of TGA changed smoothly, followed by another sharp drop in the weight of sacrificial concrete at about 1200 ºC due to the melting of cement. In addition, the weight loss of FCG was slightly lower than that of FC in the range of 25-1300 ºC. The total weight loss of FC and FCG up to 1300 ºC was 7.64% and 6.62%, respectively.

As shown in Fig.8b, the DSC patterns of FC and FCG were also close to each other that is similar to the TGA curves, since the hydration products of them were essentially the same. The dehydration of sacrificial concrete occurred at about 100 ºC characterised by the loss of evaporable water and part of physically bound water and the decomposition of calcium hydroxide took place in the range of 400-600 ºC, which are in good agreement with the results presented in [49]. At approximately 580 ºC, the crystalline of quartz transformed from α to β quartz and the decarbonation of calcium carbonate occurred at about 700 ºC, which is consistent with the conclusion drawn by Bazant and Kaplan [49] that the decomposition of calcium carbonate happens in the range of 600-900 ºC. The melting of cement was observed at approximately 1200 ºC that is in accordance with experimental results presented in [37]. It is worth pointing out that the dehydration of hydrates is generally an ongoing process between 100 ºC and 850 ºC.

3.6 Coefficient of thermal expansion

Fig.9 shows the thermal strain of sacrificial concrete without and with GSNSs. The thermal strain of sacrificial concrete increased continually with the increase of temperature. There was a sharp increase in the thermal strain in the range of 25-600 ºC followed by a gradual increase after 600 ºC. The thermal strain of sacrificial concrete at elevated temperatures can result from different aspects. Accordingly, the mechanical properties of sacrificial concrete may degrade under these circumstances [41]. The loss of water in hydration products may lead to shrinkage of concrete [50]. The siliceous aggregates containing quartz can cause inner expansive force in concrete at about 580 ºC due to the

transformation of quartz from α to β (see Fig.8b) and thus lead to volumetric expansion of sacrificial concrete. This transformation was also observed in this work that resulted in a sudden increase in the thermal strain after 580 ℃ for both FC and FCG, as shown in Fig.9. The thermal strain of FC and FCG was almost the same in the range of 25-700 ℃ because of their similar mixtures (see Table 4). However, the thermal strain of FC tended to be higher than that of FCG after 700 ℃. This may be attributed to the relatively lower thermal gradient and thermal damage in FCG than those in FC above 700 ℃ due to the addition of GSNSs. The thermal strain of FC and FCG at 600 ℃ was found to be 13.32×10^{-3} and 13.55×10^{-3}, respectively.

Fig.10 shows the first derivation of the thermal strain curves represents the phase changes on the specimens during high temperatures [51]. The first trough appeared at about 170 ℃, which may correspond to the melting of polypropylene fibres in sacrificial concrete. Two significant peaks in the curves emerged at approximately 580 ℃, which can be associated with the transformation of quartz from α to β, as discussed in the experimental results of DSC (see Fig.8b). The other weak trough occurred at around 900 ℃, where the free calcium hydroxide turned into calcium oxide.

The CTE of sacrificial concrete without and with GSNSs, i.e., FC and FCG, can be calculated using Eq. (3) and is shown in Fig.11. The CTE evolution of FC and FCG was very close, which agrees very well with the results of thermal strain as shown in Fig.9. A rapid increase in the CTE of sacrificial concrete was observed in the range of 25-150 ℃ followed by a slight drop between 150 ℃ and 200 ℃ due to the evaporation of internal free water in calcium silicate hydrate (C-S-H) gel [51]. After that, the CTE increased continually and then decreased until 1000 ℃. The CTE of sacrificial concrete reached its maximum at about 600 ℃. The increase of CTE with increasing temperature from 250 ℃ to 500 ℃ can be attributed to the decomposition of C-S-H gel. As temperature increased, the water evaporated from sacrificial concrete leading to the shrinkage of matrix, and the CTE of sacrificial

concrete decreased accordingly. However, the CTE of sacrificial concrete increased significantly between 550 ºC and 600 ºC, which can be explained by the transformation of quartz at about 580 ºC (see Figs.8b and 10). After 600 ºC, the CTE of FC and FCG reduced gradually. Overall, the CTE of sacrificial concrete was found to be in the range 1.0×10^{-5} and 2.39×10^{-5} 1/ºC, which is consistent with that of self-consolidating concrete subjected to elevated temperatures [51].

In addition, the CTE of FCG was always lower than that of FC above 700 ºC, which indicated that the addition of GSNSs to sacrificial concrete caused a reduction in its CTE. This is because the thermal gradient and thermal damage of sacrificial concrete can be reduced due to the high thermal conductivity of graphene and its derivatives, e.g., GSNSs [16]. Unlike the self-consolidating concrete as presented in [51], the CTE of sacrificial concrete did not decline suddenly, which suggested that the high temperature integrity of sacrificial concrete was higher than that of self-consolidating concrete. Moreover, the elevated temperature integrity of FCG was higher than that of FC after 700 ºC, which implied that the addition of GSNSs to sacrificial concrete could enhance its high temperature integrity.

3.7 Density

Based on the results of TGA and CTE, the mass loss ratio and volumetric CTE of sacrificial concrete can be obtained and are shown in Table 5. Fig.12 shows the density evolution of sacrificial concrete at elevated temperatures that was obtained using Eq. (7). The evolution of density for FC and FCG over temperature was similar, which is consistent with the weight evolution as shown in Fig.8a. There was a dramatic decrease in density when temperature changed from 25 ºC to 200 ºC, followed by a slightly less decrease in the range of 400-800 ºC and a gradual drop in the range of 800-1000 ºC. Over the whole range of 25-1000 ºC, the density of FCG was higher than that of FC, which corresponded with the weight evolution as discussed above. In detail, the density of FCG at

25, 600, and 1000 ºC was, 0.26%, 0.54% and 0.87% respectively higher than that of FC.

3.8 Thermal diffusivity

The thermal conductivity and the specific heat of sacrificial concrete without and with GSNSs at ambient and elevated temperatures were obtained simultaneously by mean of laser thermal constant analyzer, the results of which are presented in Table 6. Based on the obtained density of sacrificial concrete at ambient and each target temperature, the thermal diffusivity of sacrificial concrete could be calculated using Eq. (5), which is shown in Table 6 as well and is plotted in detail in Fig.13. The thermal diffusivity of sacrificial concrete decreased with increasing temperature reaching the minimum at 600 ºC and then increased with the increase of temperature. In general, the thermal diffusivity of sacrificial concrete ranged from 0.29 to 1.36 mm^2/s between ambient temperature and 1000 ºC. In addition, the thermal diffusivity of FCG was always higher than that of FC in the range of 25-1000 ºC. It can be found that the thermal diffusivity of sacrificial concrete was increased by 25.00-103.23% due to the incorporation of GSNSs. For example, the thermal diffusivity of FCG at 25, 600 and 1000 ºC was 30.77%, 68.97% and 52.50% higher than that of FC, respectively.

The higher thermal diffusivity of sacrificial concrete can help reduce its thermal gradient and thus diminish its thermal damage at high temperatures. These might explain why the residual compressive strength and splitting tensile strength of FCG were higher than that of FC over the whole range of 25-1000 ºC, as shown in Sections 3.3 and 3.4. As temperature increased, the thermal diffusivity of sacrificial concrete in the range of 25-600 ºC decreased, which can be attributed to the evaporation of water, decomposition of hydrates and thermal cracks induced by high temperatures. These explanations have been already identified by previous studies [30, 49, 52]. When the temperature was higher than 600 ºC, the microstructure of sacrificial concrete was further deteriorated (see Fig. 2) and the porosity and damage were further increased, which resulted in the increase of thermal conductivity

and specific heat, and the decrease of density. However, the increasing amplitude of thermal conductivity was higher than that of specific heat (see Table 6). Accordingly, the thermal diffusivity of sacrificial concrete tended to increase in the range of 600-1000 ºC.

It is worth noting that the aggregate type is the most important factor that affects the CTE of concrete [53]. Similar to the CTE of concrete, the thermal diffusivity of concrete may also be affected by the types and content of aggregates. However, the types and content of aggregates used in sacrificial concrete are basically fixed [29], thus the CTE and thermal diffusivity of sacrificial concrete obtained in the paper are reasonable.

3.9 Ablation behaviour

From the high temperature test through electrically furnace, the decomposition temperature of sacrificial concrete was found to be about 1120 ºC. Fig.14 shows the enthalpy of sacrificial concrete that was obtained from the DSC results presented in Fig. 8b. As temperature increased, the enthalpy of sacrificial concrete increased gradually followed by a sharp rise. The enthalpy of FCG was higher than that of FC in the range of 25-1200 ºC, while a contrary tendency can be observed after 1200 ºC, which is in accordance with the DSC results (see Fig. 8b). The decomposition enthalpy of FC and FCG was found to be 489.61 kJ/kg and 510.32 kJ/kg, respectively. The latter was 4.23% higher that of the former. It can be seen from the definition of ablation velocity that the ablation velocity is directly proportional to heat flux, but inversely proportional to density, ablating area and decomposition enthalpy. Since the density and decomposition enthalpy of FCG were always higher than those of FC (see Figs. 12 and 14), the ablation velocity of FCG was lower than that of FC for the identical heat flux and ablating area. Compared to FC, the ablation velocity of FCG was reduced by 4.14% due to the incorporation of GSNSs, which implied that the melt-through time of basemat can be prolonged and thus the safety of nuclear power plant can be enhanced in severe nuclear

accident by adding GSNSs to sacrificial concrete.

4. Conclusions

In this study, the mechanical and thermal properties of ferro-siliceous sacrificial concrete without and with GSNSs (i.e., FC and FCG) at high temperatures were investigated. Two new experimental facilities for measuring compressive strength and splitting tensile strength sacrificial concrete during elevated temperature exposure were developed and used. Based on the findings of this study, the following conclusions can be drawn:

- GSNSs had reinforcing and toughing effects on the microstructure of sacrificial concrete. The porosity of sacrificial concrete increased continually with increasing temperature. The porosity of sacrificial concrete was reduced by 3.01-6.99% due to the addition of GSNSs.

- The compressive strength and splitting tensile strength of sacrificial concrete decreased monotonically with the increase of temperature. For FCG, its compressive strength and splitting tensile strength were always higher than those of FC in the whole range of 25-1000 ℃. Because of the incorporation of GSNSs, the compressive strength and splitting tensile strength of sacrificial concrete were increased by 12.98-25.36% and 8.66-34.38%, respectively.

- The weight evolution of FC and FCG was similar, while weight loss of FCG is lower than that of FC in the range of 25-1300 ℃. The total weight loss of FC and FCG up to 1300 ℃ was 7.64% and 6.62%, respectively.

- The thermal strain of sacrificial concrete increased dramatically in the range of 25-600 ℃ followed by a gradual increase after 600 ℃. The thermal strain of FC and FCG was almost the same in the range of 25-700 ℃, while the thermal strain of FCG was lower than that of FC after 700 ℃ due to the addition of GSNSs.

- The coefficient of thermal expansion (CTE) of sacrificial concrete was found to be within the range

of 1.0×10^{-5} and 2.39×10^{-5} 1/ºC. The elevated temperature integrity of FCG was higher than that of FC after 700 ºC, which suggested that the addition of GSNSs to sacrificial concrete can enhance its high temperature integrity.

- The thermal diffusivity of sacrificial concrete decreased as temperature increased from ambient temperature to 600 ºC and then increased with increasing temperature. The thermal diffusivity of sacrificial concrete was increased by 25.00-103.23% due to the incorporation of GSNSs.

- The decomposition enthalpy of FCG was 4.23% higher that of FC and the ablation velocity of sacrificial concrete was reduced by 4.14% due to the incorporation of GSNSs, as such the safety of nuclear power plant can be improved by adding GSNSs to sacrificial concrete.

Acknowledgements

References

[1] C. Nunes, Z. Slizkova, M. Stefanidou, J. Nemecek, Microstructure of lime and lime-pozzolana pastes with nanosilica, Cem. Concr. Res. 83 (2016) 152-163.

[2] M. Nili, A. Ehsani, Investigating the effect of the cement paste and transition zone on strength development of concrete containing nanosilica and silica fume, Mater. Des. 75 (2015) 174-183.

[3] P. Hou, K. Wang, J. Qian, S. Kawashima, D. Kong, S.P. Shah, Effects of colloidal nanoSiO$_2$ on fly ash hydration, Cem. Concr. Compos. 34 (2012) 1095-1103.

[4] T. Menga, Y. Yub, X. Qiana, S. Zhana, K. Qiana, Effect of nano-TiO$_2$ on the mechanical properties of cement mortar, Constr. Build. Mater. 29 (2012) 241-245.

[5] E. Mohseni, M.M. Khotbehsara, F. Naseri, M. Monazami, P. Sarker, Polypropylene fibre reinforced cement mortars containing rice husk ash and nano-alumina, Constr. Build. Mater. 111 (2016) 429-439.

[6] K. Behfarnia, N. Salemi, The effects of nano-silica and nano- alumina of frost resistance of normal concrete, Constr. Build. Mater. 48 (2013) 580-584.

[7] M.O.G.P. Braganca, K.F. Portella, M.M. Bonato, E. Alberti, C.E.B. Marino, Performance of Portland cement concretes with 1% nano-Fe$_3$O$_4$ addition: electrochemical stability under chloride and sulfate environments, Constr. Build. Mater. 117 (2016) 152-162.

[8] A.D'Alessandro, M. Rallini, F. Ubertini, A.L. Materazzi, J. M. Kenny, Investigation on scalable fabrication procedures for self-sensing carbon nanotube cement-matrix composites for SHM applications, Cem. Concr. Compos. 65 (2016) 200-213.

[9] S. Parveen, S. Rana, R. Fangueiro, M.C. Paiva, Microstructure and mechanical properties of carbon nanotube reinforced cementitious composites developed using a novel dispersion technique, Cem. Concr. Res. 73 (2015) 215-227.

[10] S.M.H. Farrash, M. Shariati, J. Rezaeepazhand, The effect of carbon nanotube dispersion on the dynamic characteristics of unidirectional hybrid composites: An experimental approach, Compos. Part B Eng. 122 (2017) 1-8.

[11] P. Hou, S. Kawashima, D. Kong, D.J. Corr, J. Qian, S.P. Shah, Modification effects of colloidal nanoSiO$_2$ on cement hydration and its gel property, Compos. Part B Eng. 45 (2013) 440-448.

[12] S. Lv, L. Deng, W. Yang, Q. Zhou, Y. Cui, Fabrication of polycarboxylate/graphene oxide nanosheet composites by copolymerization for reinforcing and toughening cement composites,

Cem. Concr. Compos. 66 (2016) 1-9.

[13] D. Hou, Z. Lu, X. Li, H. Ma, Z. Li, Reactive molecular dynamics and experimental study of graphenecement composites: Structure, dynamics and reinforcement mechanisms, Carbon 115 (2017)188-208.

[14] K.S. Novoselov, A.K. Geim, S.V. Morozov, D. Jiang, M. Katsnelson, I. Grigorieva, A. Firsov, Two-dimensional gas of massless Dirac fermions in graphene, Nature 438 (7065) (2005) 197-200.

[15] V. Singh, D. Joung, L. Zhai, S. Das, S.I. Khondaker, S. Seal, Graphene based materials: past, present and future, Prog. Mater. Sci. 56 (8) (2011) 1178-1271.

[16] A.K. Geim, K.S. Novoselov, The rise of graphene, Nat. Mater. 6 (2007) 183-191.

[17] W. Lv, Z. Li, Y. Deng, Q. Yang, F. Kang, Graphene-based materials for electrochemical energy storage devices: Opportunities and challenges, Energy Storage Mater. 2 (2016) 107-138.

[18] Z. Pan, L. He, L. Qiu, A.H. Korayem, G. Li, J.W. Zhu, F. Collins, D. Li, W.H. Duan, M.C. Wang, Mechanical properties and microstructure of a graphene oxide-cement composite, Cem. Concr. Compos. 58 (2015) 140-147.

[19] V. Chabot, D. Higgins, A. Yu, X. Xiao, Z. Chen, J. Zhang, A review of graphene and graphene oxide sponge: material synthesis and applications to energy and the environment, Energy Environ. Sci. 7 (5) (2014) 1564-1596.

[20] J.L. Le, H. Du, S.D. Pang, Use of 2D graphene nanoplatelets (GNP) in cement composites for structural health evaluation, Compos. Part B Eng. 67 (2014) 555-563.

[21] Y. Zhu, S. Murali, W. Cai, X. Li, J.W. Suk, J.R. Potts, R.S. Ruoff, Graphene and graphene oxide: synthesis, properties, and applications, Adv. Mater. 22 (35) (2010) 3906-3924.

[22] J. Kim, L.J. Cote, F. Kim, W. Yuan, K.R. Shull, J. Huang, Graphene oxide sheets at inerfaces, J.

Am. Chem. Soc. 132 (23) (2010) 8180-8186.

[23] E. Horszczaryk, E. Mijowska, R.J. Kalenczuk, M. Aleksandrzak, S. Mijowska, Nanocomposite of cement/graphene oxide – impact on hydration kinetics and Young's modulus, Constr. Build. Mater. 78 (2015) 234-242.

[24] M. Bulut, Mechanical characterization of Basalt/epoxy composite laminates containing graphene nanopellets, Compos. Part B Eng. 122 (2017) 71-78.

[25] M. Murugan, M. Santhanam, S.S. Gupta, T. Pradeep, S.P. Shah, Influence of 2D rGO nanosheets on the properties of OPC paste, Cem. Concr. Compos. 70 (2016) 48-59.

[26] Z. Lu, D. Hou, L. Meng, G. Sun, C. Lu, Z. Li, Mechanism of cement paste reinforced by graphene oxide/carbon nanotubes composites with enhanced mechanical properties, RSC Adv. 5 (2015) 100598-100605.

[27] H. Chu, J. Chen, The experimental study on the correlation of resistivity and damage for conductive concrete, Cem. Concr. Compos. 67 (2016) 12-19.

[28] H. Chu, J. Jiang, W. Sun, M. Zhang, Thermal behaviour of siliceous and ferro-siliceous sacrificial concrete subjected to elevated temperatures, Mater. Des. 95 (2016) 470-480.

[29] R.J.M. Konings, T.R. Allen, R.E. Stoller, S. Yamanaka, Comprehensive nuclear materials. Amsterdam: Elsevier. 2012.

[30] S.C. Kou, C.S. Poon, M. Etxeberria, Residue strength, water absorption and pore size distributions of recycled aggregate concrete after exposure to elevated temperatures, Cem. Concr. Compos. 53 (2014) 73-82.

[31] H. Fares, A. Noumowe, S. Remond, Self-consolidating concrete subjected to high temperature mechanical and physicochemical properties, Cem. Concr. Res. 39 (2009) 1230-1238.

[32] F.L. Monte, P.G. Gambarova, Thermo-mechanical behaviour of baritic concrete exposed to high

temperature, Cem. Concr. Compos. 53 (2014) 305-315.

[33] A. Behnood, H. Ziari, Effects of silica fume addition and water to cement ratio on the properties of high-strength concrete after exposure to high temperatures, Cem. Concr. Compos. 30 (2008) 106-112.

[34] Z. Pan, J.G. Sanjayan, F. Collins, Effect of transient creep on compressive strength of geopolymer concrete for elevated temperature exposure, Cem. Concr. Res. 56 (2014) 182-189.

[35] H. Chu, J. Jiang, W. Sun, M. Zhang, Mechanical and physicochemical properties of ferro-siliceous concrete subjected to elevated temperatures, Constr. Build. Mater. 122 (2016) 743-752.

[36] H.-y. Chu, J.-y. Jiang, W. Sun, M. Zhang, Effect of graphene sulfonate nanosheets on mechanical and thermal properties of sacrificial concrete during high temperature exposure, Cem. Concr. Compos. 82 (2017) 252-264.

[37] M.W. Chase, NIST-JANAF Thermochemical Tables, Journal of Physical and Chemical Reference Data, Monograph 9, fourth ed., Springer, Berlin, 1998.

[38] L.T. Phan, N.J. Carino, Effects of test conditions and mixture proportions on behaviour of high-strength concrete exposed to high temperatures, ACI Mater. J. 99 (1) (2002) 54-66.

[39] F.J. Ulm, O. Coussy, Z.P. Bazant, The chunnel fire: chemoplastic softening in rapidly heated concrete, J. Eng. Mech. 125(3) (1999) 272-282.

[40] T. Ramanathan, A.A. Abdala, S. Stankovich, D.A. Dikin, A.M. Herrera, R.D. Piner, Functionalized graphene sheets for polymer nanocomposites, Nat. Nano. 3(6) (2008) 327-331.

[41] M.J. Heap, Y. Lavallee, A. Laumann, K.U. Hess, P.G. Meredith, D.B. Dingwell, S. Huismann, F. Weise, The influence of thermal-stressing (up to 1000 ℃) on the physical, mechanical, and chemical properties of siliceous-aggregate, high-strength concrete, Constr. Build. Mater. 42 (2013) 248-265.

[42] P. Pliya, A.L. Beaucour, A. Noumowe, Contribution of cocktail of polypropylene and steel fibres in improving the behaviour of high strength concrete subjected to high temperature, Constr. Build. Mater. 25 (2011) 1926-1934.

[43] C. Galle, J. Sercombe, Permeability and pore structure evolution of silicocalcareous and hematite high-strength concretes submitted to high temperatures, Mater. Struct. 34 (2001) 619-628.

[44] H.T. Le, M. Muller, K. Siewert, H.M. Ludwig, The mix design for self-compacting high performance concrete containing various mineral admixtures, Mater. Des. 72 (2015) 51-62.

[45] A.S. El-Dieb, Mechanical, durability and microstructural characteristics of ultra-high-strength self-compacting concrete incorporating steel fibres, Mater. Des. 30 (2009) 4286-4292.

[46] D. Hou, D. LI, T. Zhao, Z. Li, Confined water dissociation in disordered silicate nanometer-channels at elevated temperatures: mechanism, dynamics and impact on substrates, Langmuir, 32 (2016) 4153-4168.

[47] A. Behnood, M. Ghandehari, Comparison of compressive and splitting tensile strength of high-strength concrete with and without polypropylene fibres heated to high temperatures, Fire Saf. J. 44 (2009) 1015-1022.

[48] G. Ye, X. Liu, D.G. Schutter, Phase distribution and microstructural changes of self-compacting cement paste at elevated temperature, Cem. Concr. Res. 37(6) (2007) 978-987.

[49] Z.P. Bazant, M.F. Kaplan, Concrete at High Temperatures: Materials Properties and Mathematical Models, Longman, London, 1996.

[50] L. Zuda, R. Cerny, Measurement of linear thermal expansion coefficient of alkali-activated aluminaosilicate composites up to 1000 ºC, Cem. Concr. Compos. 31(4) (2009) 263-267.

[51] T. Uygunoglu, I.B. Topcu, Thermal expansion of self-consolidating normal and lightweight aggregate concrete at elevated temperature, Constr. Build. Mater. 23 (2009) 3063-3069.

[52] Z. Xing, A.L. Beaucour, R. hebert, A. Noumowe, B. Ledesert, Influence of the nature of aggregates on the behaviour of concrete subjected elevated temperature, Cem. Concr. Res. 41 (2011) 392-402.

[53] C. Zhou, X. Shu, B. Huang, Predicting concrete coefficient of thermal expansion with an improved micromechanical model, Constr. Build. Mater. 68 (2014) 10-16.

Table 1 Chemical composition of cement and supplementary cementitious materials (wt%)

Materials	Cement	Silica fume	Fly ash
CaO	64.70	0.77	8.38
SiO_2	20.40	96.18	47.96
Al_2O_3	4.70	0.96	30.46
Fe_2O_3	3.38	0.85	5.91
MgO	0.87	0.74	2.60
SO_3	1.88	0.50	1.32
K_2O	0.83		1.61
Na_2O			1.76
Loss	3.24		

Table 2 Particle size distribution of the aggregates (wt%)

Particle size (mm)	0-0.15	0.15-0.30	0.30-0.63	0.63-2.36	2.36-4.75	4.75-8.00
Silica sand	6.30	7.60	13.50	14.60	11.50	46.50
Iron ore	5.20	7.10	12.70	39.00	17.80	18.20

Table 3 Physical and mechanical properties of polypropylene fibre

Technical specification	Polypropylene fibre
Purity (%)	100
Length (mm)	12
Diameter (μm)	18
Density (kg/m^3)	910
Melting temperature (^{o}C)	169
Burning temperature (^{o}C)	590
Young's modulus (MPa)	>3500
Tensile strength (MPa)	386
Elongation at yield (%)	16

Table 4 Mix proportions of sacrificial concrete (kg/m^3)

Mixture	FC	FCG
Cement	388	388
Fly ash	135	135
Silica fume	20.0	20.0
Iron ore (0-4 mm)	764	764
Iron ore (4-8 mm)	216	216
Silica sand (0-5 mm)	594	594
Silica sand (5-8 mm)	466	466
Water	181	181
Superplasticizer	8.00	8.00
Polypropylene fibres	1.40	1.40
GSNSs	0	0.543

Table 5 Mass loss ratio and volumetric coefficient of thermal expansion of sacrificial concrete

Temperature (ºC)	Mass loss ratio (γ) $\times 10^{-2}$		Volumetric CTE (β) $\times 10^{-5}$	
	FC	FCG	FC	FCG
25	0	0	0	0
200	2.38	2.12	3.40	3.12
400	3.43	3.08	4.75	4.64
600	4.32	4.04	7.31	7.15
800	6.03	5.42	5.57	5.34
1000	6.18	5.61	4.52	4.28

Table 6 Thermal properties of sacrificial concrete before and during exposure to elevated temperatures

Temperature (ºC)	Thermal conductivity [W/(m·K)]		Specific heat [J/(g·K)]		Thermal diffusivity (mm^2/s)	
	FC	FCG	FC	FCG	FC	FCG
25	2.09	2.56	0.75	0.70	1.04	1.36
200	1.44	1.68	0.86	0.80	0.64	0.80
400	1.06	1.56	0.95	0.82	0.43	0.73
600	0.93	1.27	1.23	1.00	0.29	0.49
800	1.05	2.07	1.45	1.08	0.31	0.63
1000	1.45	2.82	1.62	1.35	0.40	0.61
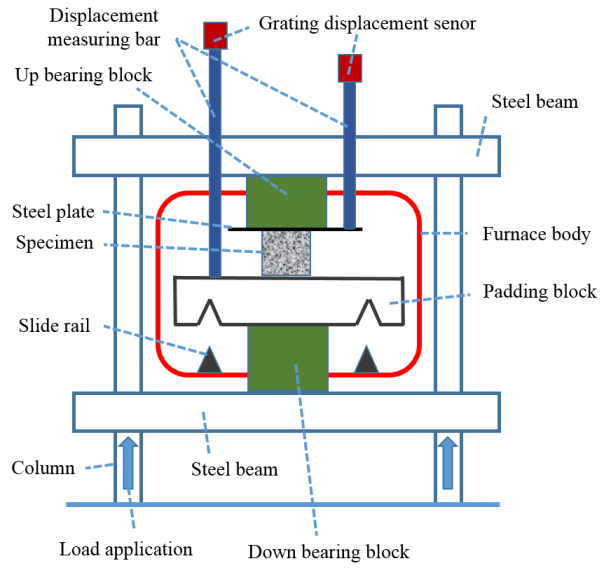
(a)
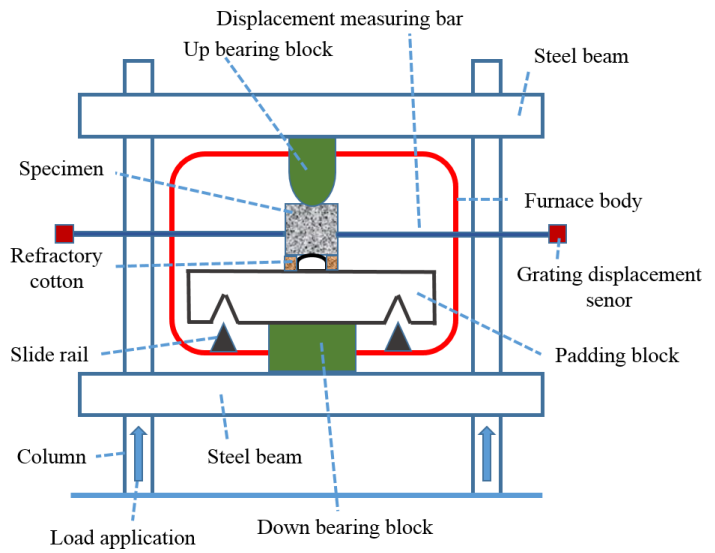
(b)

Fig. 1 New testing setups for measuring mechanical properties during exposure to high

temperatures: (a) compressive strength; (b) splitting tensile strength
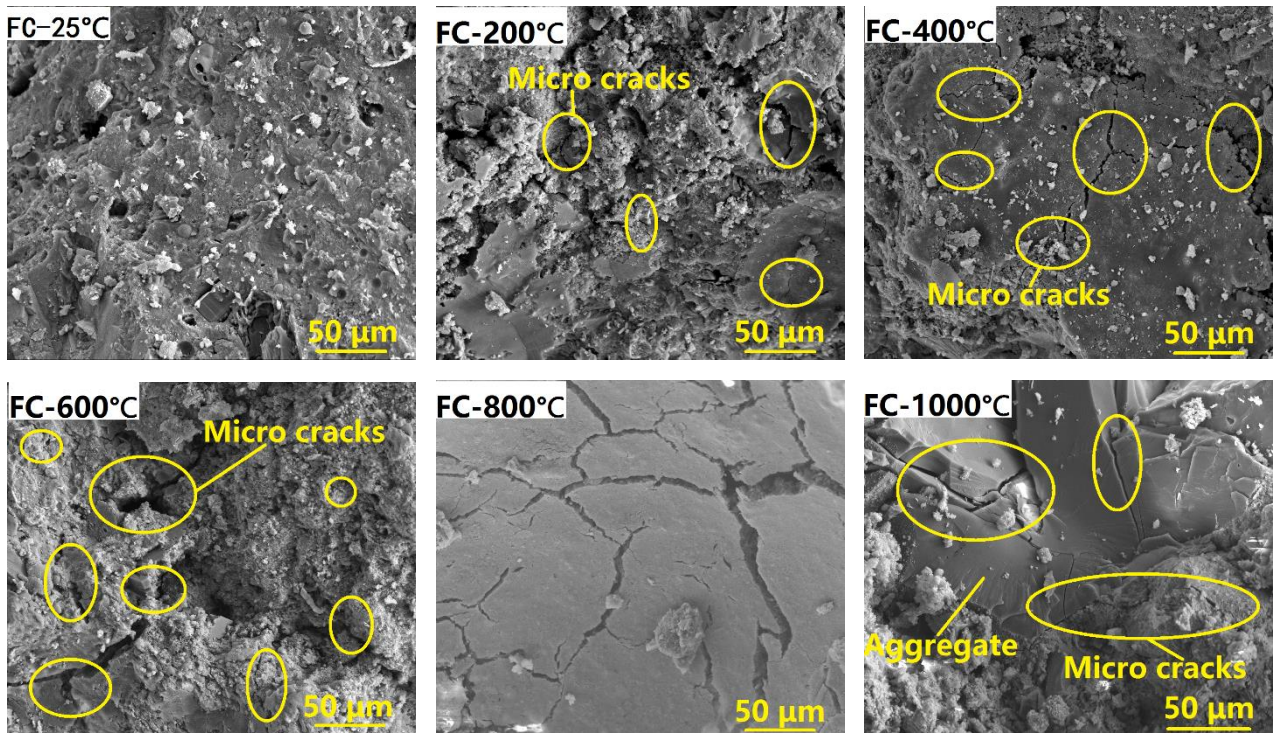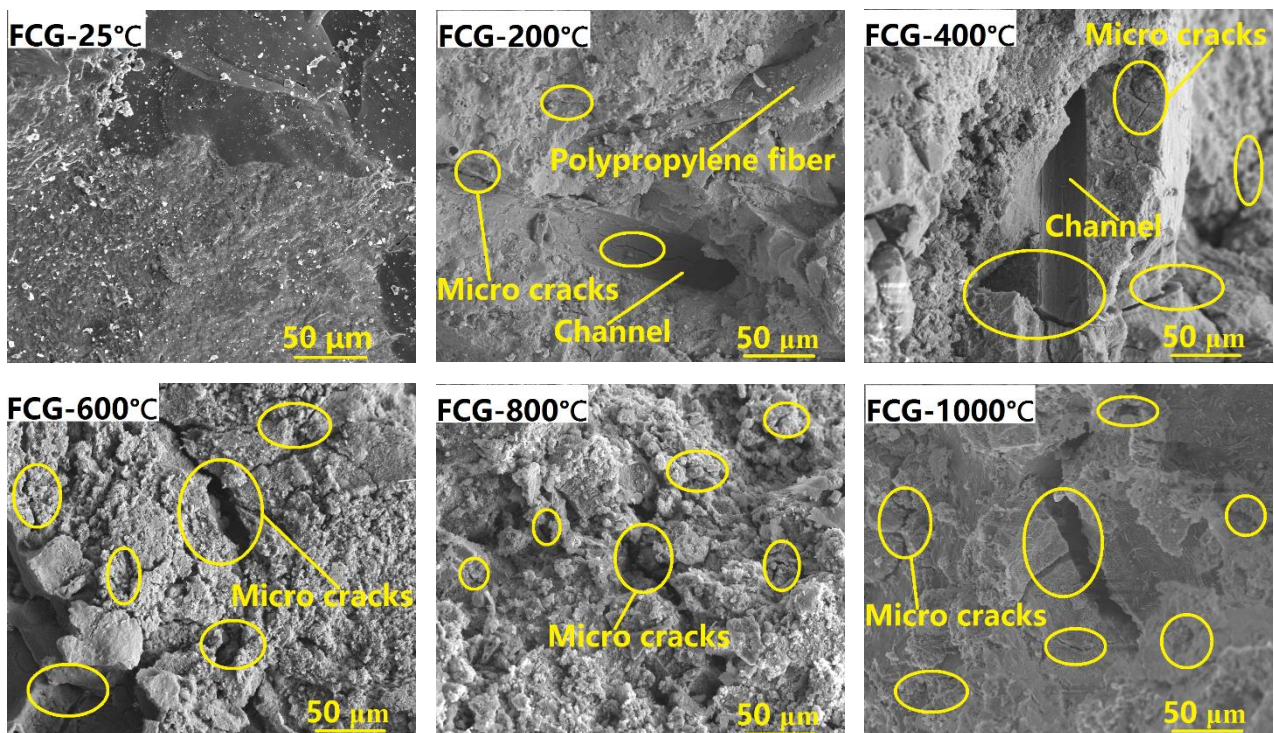
Fig. 2 ESEM images of specimens before and after exposure to different temperatures: (a) sacrificial concrete without GSNSs (FC); (b) sacrificial concrete with GSNSs (FCG)
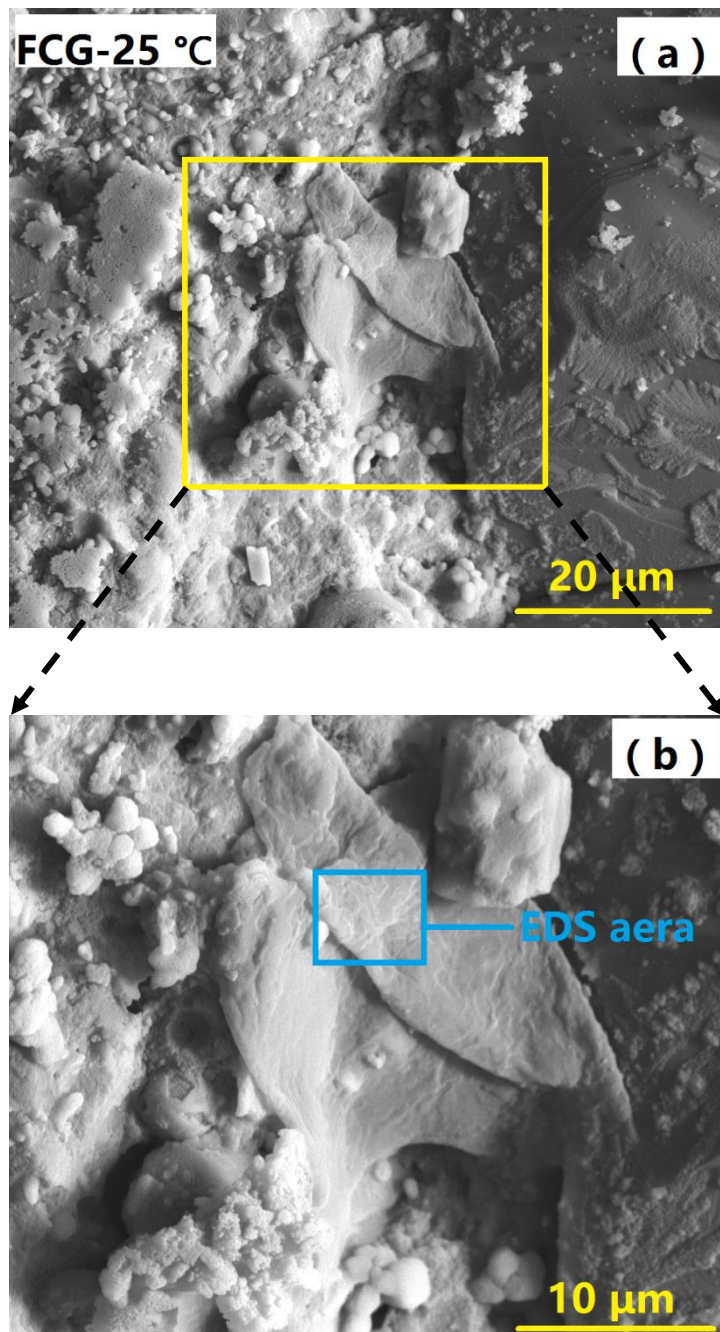
Fig. 3 Microstructure of sacrificial concrete with cumulative plate-shaped products
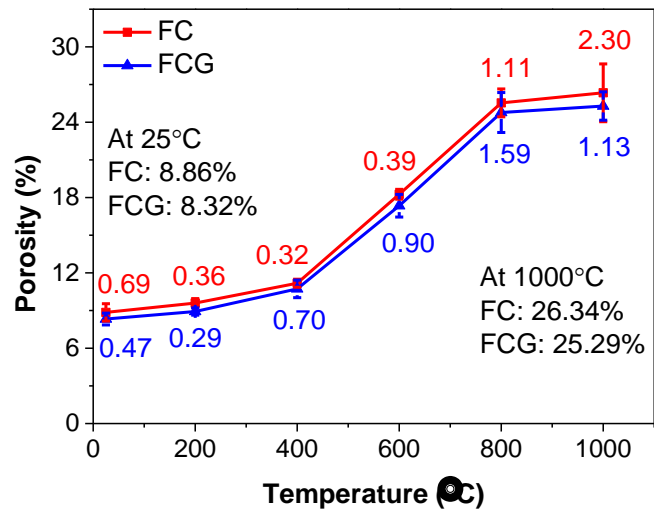
(a)
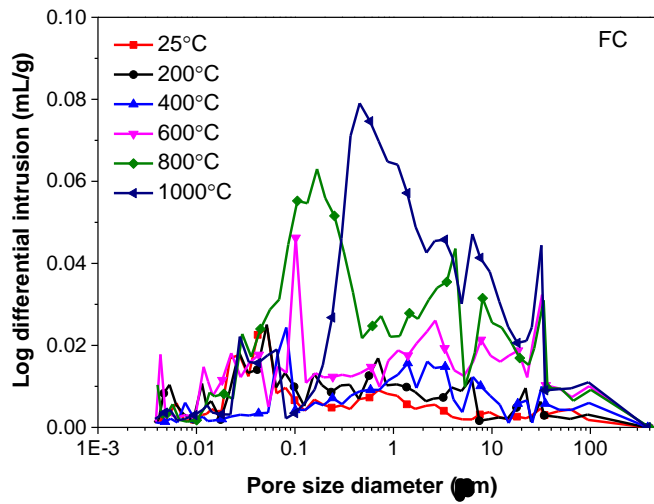
(b)
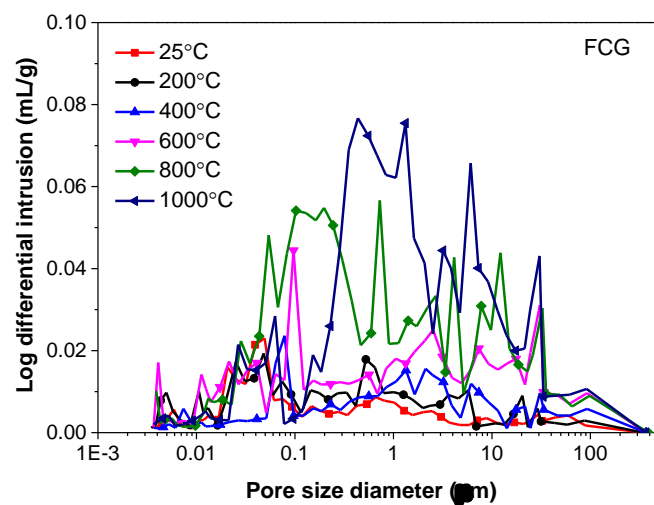
(c)

Fig. 4 Porosity and pore size distribution of sacrificial concrete after exposure to elevated temperatures: (a) porosity; (b) pore size distribution of FC; and (c) pore size distribution of FCG
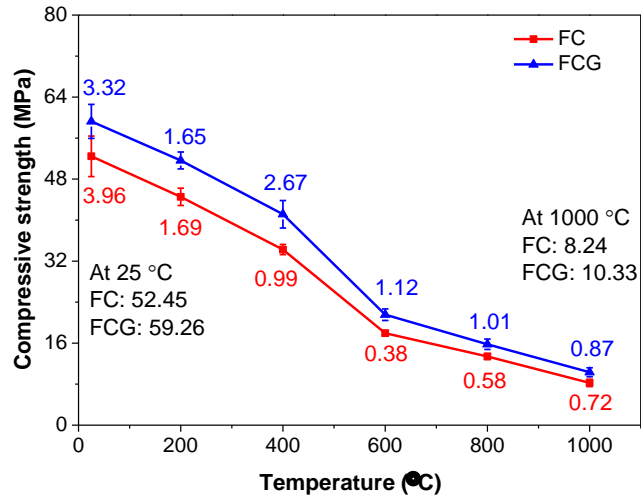
(a)
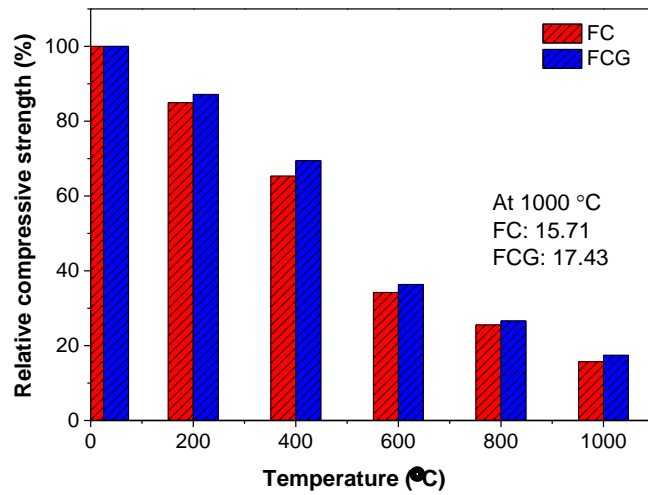
(b)

(a)

(b)

Fig. 6 Splitting tensile strength of sacrificial concrete after exposure to elevated temperatures: (a) residual splitting tensile strength; and (b) relative residual splitting tensile strength (compared to strength at 25 °C)
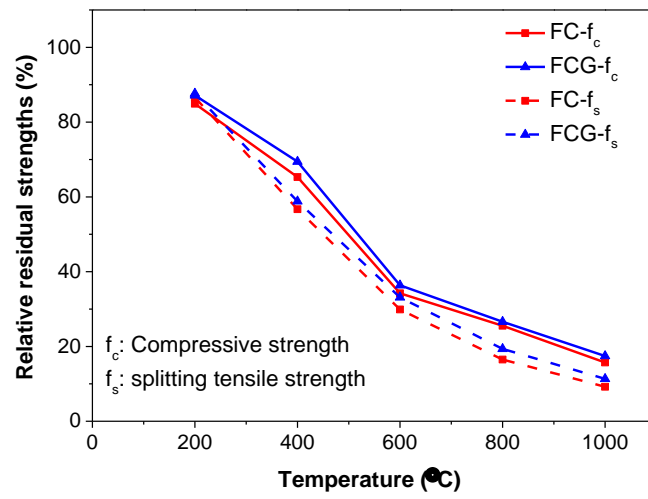
Fig. 7 Relative strength of sacrificial concrete after exposure to elevated temperatures
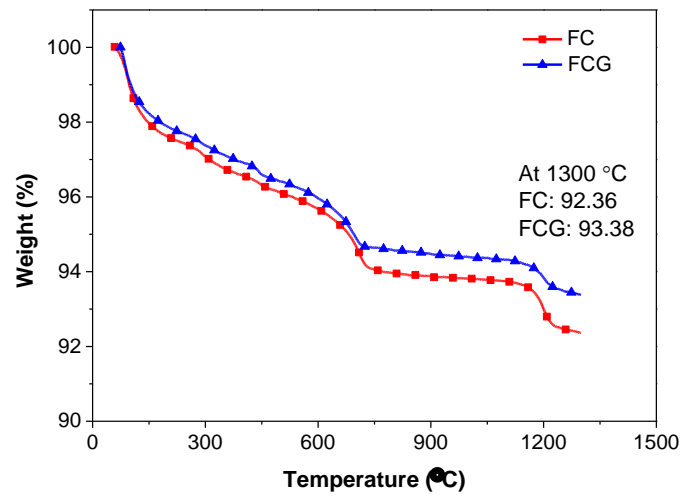
(a)
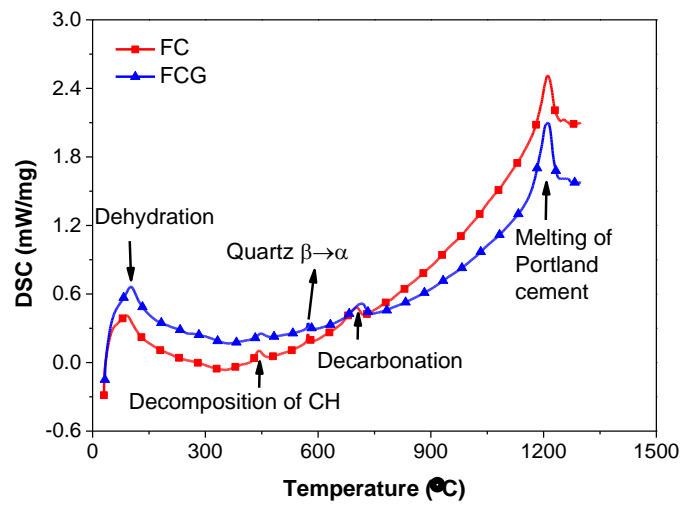
(b)

Fig. 8 Thermal analysis of sacrificial concrete: (a) TGA curves; and (b) DSC spectrums
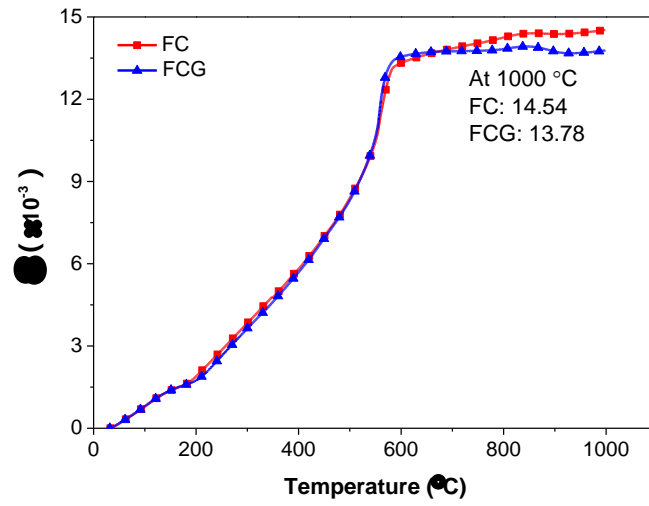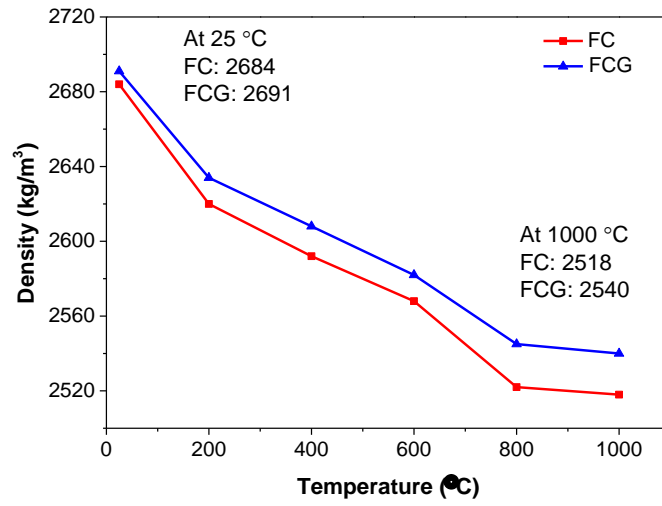
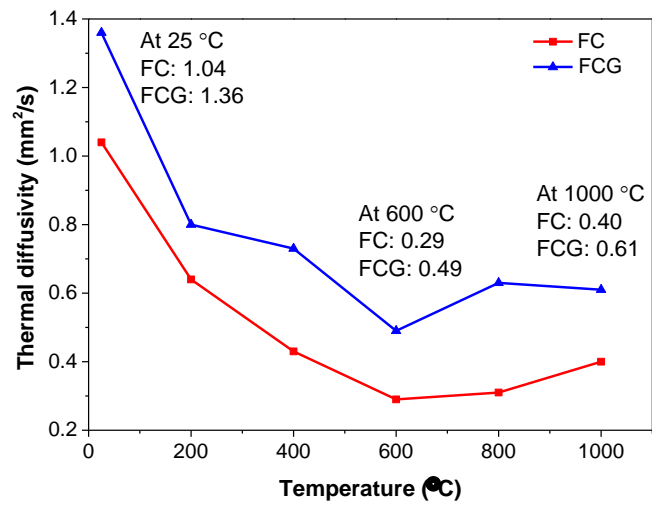**Fig. 9** Thermal strain of sacrificial concrete without and with GSNSs
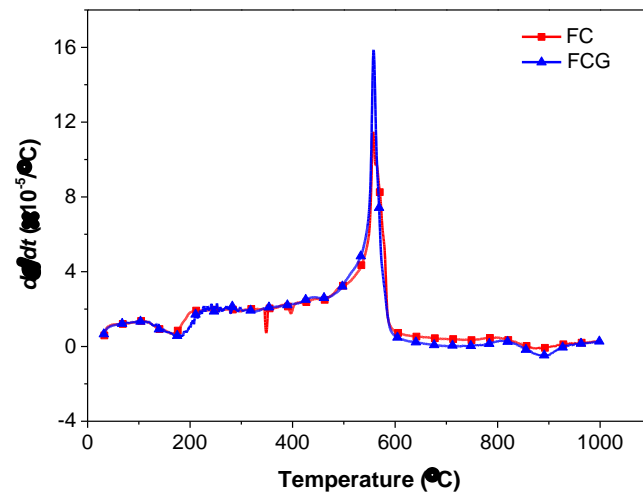
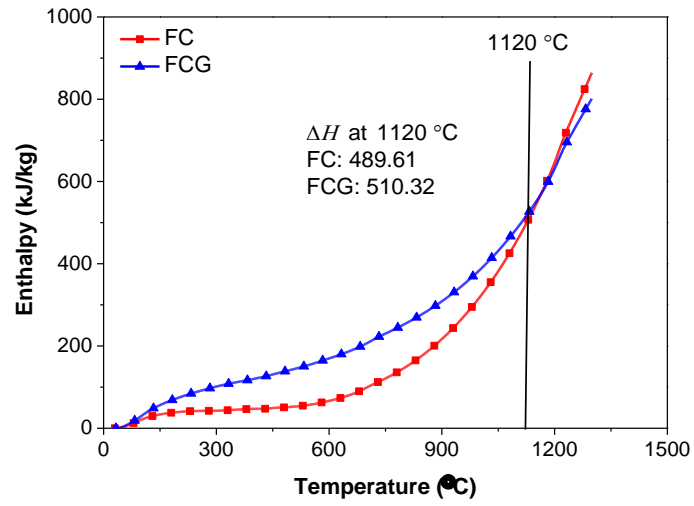**Fig. 10** First derivation of thermal strain of sacrificial concrete without and with GSNSs
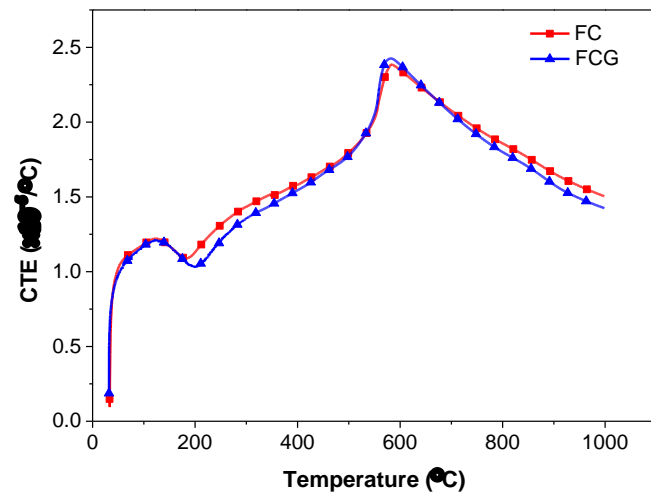
Fig. 11 Coefficient of thermal expansion of sacrificial concrete without and with GSNSs

Fig. 12 Density evolution of sacrificial concrete without and with GSNSs

Fig. 13 Thermal diffusivity of sacrificial concrete without and with GSNSs

Fig. 14 Enthalpy and decomposition enthalpy (at 1120 ºC) of sacrificial concrete without and with

GSNSs